Single-Molecule Recognition of Biomolecular Interaction *via* Kelvin Probe Force Microscopy

Jinsung Park,[†,‡,#] Jaemoon Yang,[†,§,#] Gyudo Lee,[†,⊥] Chang Young Lee,[∥] Sungsoo Na,[‡] Sang Woo Lee,[⊥] Seungjoo Haam,[¶] Yong-Min Huh,[§] Dae Sung Yoon,[⊥] Kilho Eom,[†,‡,*] and Taeyun Kwon[†,⊥,*]

[†]Institute for Molecular Sciences, Seoul 120-749, Republic of Korea, [‡]Department of Mechanical Engineering, Korea University, Seoul 136-701, Republic of Korea, [§]Department of Radiology, Yonsei University, Seoul 120-752, Republic of Korea, [⊥]Department of Biomedical Engineering, Yonsei University, Wonju 220-740, Republic of Korea, [∥]Department of Chemistry, University of Illinois at Urbana—Champaign, Urbana, Illinois 61801, United States, and [¶]Department of Chemical and Biomolecular Engineering, Yonsei University, Seoul 120-749, Republic of Korea. [#]These authors contributed equally to this work.

ABSTRACT We report the scanning probe microscope (SPM)-based single-molecule recognition of biomolecular interactions between protein kinase and small ligands (*i.e.*, ATP and Imatinib). In general, it is difficult to sense and detect the small ligands bound to protein kinase (at single-molecule resolution) using a conventional atomic force microscope (AFM) due to the limited resolution of conventional AFM for detecting the miniscule changes in molecular size driven by ligand binding. In this study, we have demonstrated that Kelvin probe force microscopy (KPFM) is able to articulate the surface potential of biomolecules interacting with ligands (*i.e.*, the protein kinase—ATP interactions and inhibition phenomena induced by antagonistic molecules) in a label-free manner. Furthermore, measured surface potentials for biomolecular interactions enable quantitative descriptions on the ability of protein kinase to interact with small ligands such as ATP or antagonistic molecules. Our study sheds light on KPFM that allows the precise recognition of single-molecule interactions, which opens a new avenue for the design and development of novel molecular therapeutics.

KEYWORDS: single molecule · biomolecular interactions · protein kinase · Kelvin probe force microscopy · label-free · surface potential

In the pathological viewpoint, cellular signaling and energy metabolism driven by protein kinase play a significant role in a cell's functions and malfunctions leading to undesirable disease expressions such as various cancers (*e.g.*, leukemia).[1−3] For the early diagnosis and effective treatment of diseases *via* nanomedicine, it is therefore requisite to develop a method that enables the fast, reliable, label-free identification of interactions between marker protein kinases and small molecules such as adenosine-5′-triphosphate (ATP) and/or inhibitors serving as drugs.[4] In particular, the quantitative identification of such interactions is necessary for fundamental insights into drug sensitivity and/or drug resistance of protein kinases, which would contribute to the development of effective personalized therapeutics.[5] Moreover, it is essential to establish the ability to visualize and characterize the proteins at multiple scales (from single-molecule scale to subcellular level) for understanding the origin of disease expression (at molecular level) as well as disease treatment.[6−9] For instance, the underlying mechanisms of interaction between a single protein and small molecule (such as ATP), which can be gained from computational simultions (*e.g.*, molecular dynamics simulations),[8,9] are essential for *de novo* drug design. Until recently, methods that allow for quantitative identification of such molecular interactions at single-molecule resolution have rarely been reported. In particular, the nanotechnology-based detection (*e.g.*, using nanowire field effect transistor[10]), albeit their ability to sense the ATP-binding events and/or small-molecule-mediated inhibition, exhibits the restrictions in that the resolution of such a detection does not reach the single-molecule level. Recognition of ATP binding or small-molecule-mediated inhibition at single-molecule resolution is necessary for gaining an insight into the regulation of signaling cascade for disease treatment,[11,12] which enables the fundamental understanding of drug sensitivity for *de novo* drug design.

In this study, we report a novel approach to identify and quantify molecular interactions at single-molecule level using a scanning probe microscopy (SPM), particularly Kelvin probe force microscopy (KFPM). In a recent decade, SPM has been widely utilized for imaging various biological samples.[4,13] For example, tapping-mode AFM (tmAFM) imaging has recently been successful in imaging biomolecules such as membrane proteins,[14−16] single DNA/RNA molecules,[4,14] and proteins[17] at

* Address correspondence to tkwon@yonsei.ac.kr, kilhoeom@korea.ac.kr.

Received for review April 27, 2011 and accepted August 1, 2011.

Published online August 01, 2011
10.1021/nn201540c

single-molecule resolution. The principle of AFM-based imaging/detection is the transduction of interaction between a biological sample and the AFM tip into the resonant frequency shifts of the AFM cantilever.[18] In addition, the AFM cantilever has recently been considered for label-free detection of various biomolecular interactions.[19,20] However, AFM-based label-free detection exhibits the limitations in that AFM does not enable the recognition of small-molecule binding onto a single protein (at single-molecule resolution) due to the restricted spatial resolution of AFM.[4,14−17,21] Recently, Kelvin probe force microscopy (KPFM) has been introducued for imaging the surface charges of protein arrays,[22] bacteriorhodopsin,[23] biomolecular monolayers,[24,25] and single proteins.[26] The principle of KPFM for imaging the surface charges of a biological sample is attributed to Lord Kelvin,[27] who first suggested the "vibrating capacitance method" to the measure a difference between the work functions of the AFM tip and sample, respectively (for details, see Methods). This implies that KPFM is a robust experimental toolkit allowing for the recognition of binding between a single protein and small molecule due to the binding-induced surface potential change that can be measured by KPFM (Figure 1). Nonetheless, as reported in literature,[22,24−26,28] KPFM has not been taken into account for a single-molecule recognition of interaction between a single protein and a small-molecule such as ATP. In this work, we have utilized KPFM for single-molecule recognition of not only the molecular binding between ATP and Abl tyrosine kinase but also binding inhibition due to Imatinib,[29] which sheds light on KPFM that offers an underlying insight into binding mechanism at single-molecule resolution for future implications in nanomedicine such as drug design.

RESULTS AND DISCUSSION

Single-Molecule Imaging of Proteins. To find the optimal conditions for imaging single molecules, the height and potential maps of Abl tyrosine kinase was obtained using tmAFM and KPFM,[30−32] respectively. In Figure 2a, an individual Abl tyrosine kinase is imaged as a red dot with its AFM height of less than 3 nm, which is consistent with previous studies,[17,26] and their size distribution was provided in Figure S1 (Supporting Information). In order to focus on an individual Abl tyrosine kinase, we have only considered individual Abl tyrosine kinases that were imaged with AFM height of ≤3 nm unless specified. To measure the surface potential of an individual Abl tyrosine kinase, we have employed lift-mode KPFM imaging technique[22,24,33] because its resolution is higher than that of dual frequency-mode KPFM imaging technique[29,34] (see also Figure S2 in Supporting Information). This implies that the KPFM image

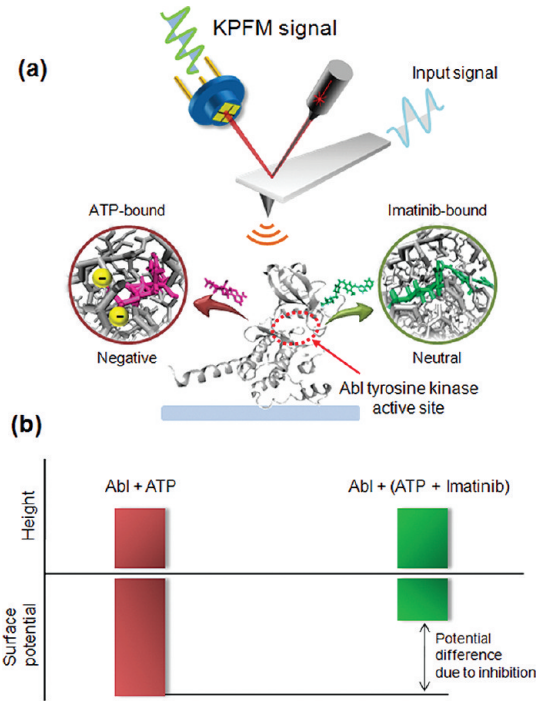

Figure 1. Schematic illustration for the identification and quantification of (a) Abl tyrosine kinase bound to ATP and (b) the Imatinib-driven inhibition of ATP binding onto Abl tyrosine kinase by using KPFM-based single-molecule imaging due to the surface potential difference.

obtained from dual frequency mode may be more significantly affected by a cross-talk than lift-mode imaging. Because imaging quality generally depends on scanning speed, we have considered KPFM images of Abl tyrosine kinases at two different scanning speeds (Figure 2b and Figure S3 in Supporting Information). The low-resolution KPFM image at a scanning speed of 15 μm/s suggests that fast scanned imaging is still challenging.[35] Further, because of the dependence of imaging quality on lift scan height, we have studied the effect of lift scan height on the surface potential profile of Abl tyrosine kinases (see Figure 2c and Figure S4 in Supporting Information). If the KPFM tip is too close to the sample, then the tip−sample interaction including the contact between tip and sample impedes the KPFM imaging, which results an underestimation of surface potential. On the other hand, if the KPFM tip is too far from the sample, measurement of surface potential is difficult since the tip−sample distance is much larger than the length scale for short-range electrostatic interactions reflected into the surface potential profile. As shown in Figure 2d, therefore, the optimal surface potential image for Abl tyrosine kinase was obtained at the lift scan height of 5 nm.

On the basis of the optimal imaging conditions as mentioned above, we have imaged Abl tyrosine kinase (MW = 45 kDa) using KPFM. As shown in Figure 3a, a single Abl tyrosine kinase can be recognized by KPFM,

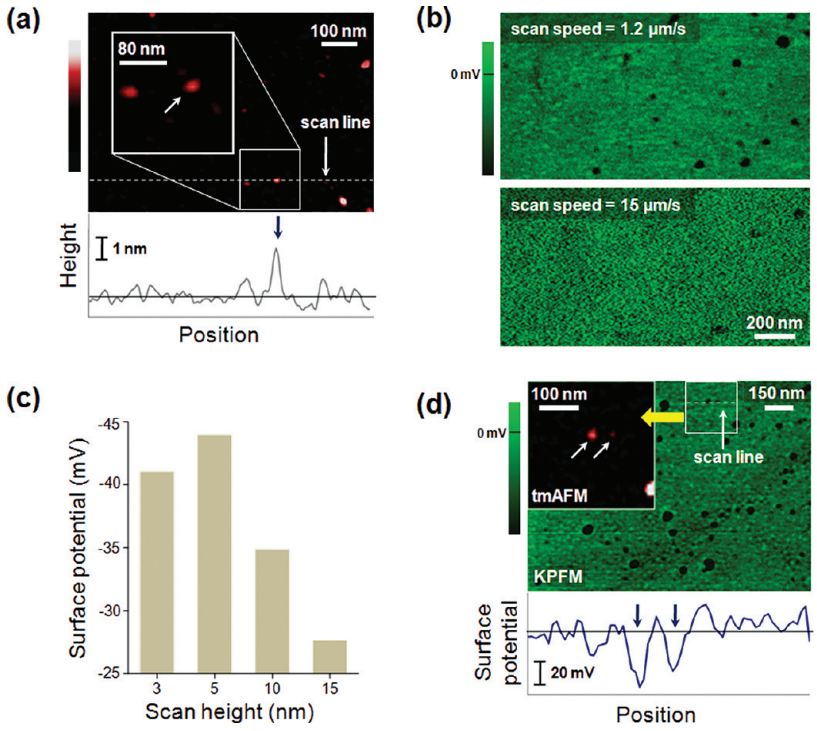

Figure 2. (a) Tapping-mode AFM image of Abl tyrosine kinase (white arrow) and their corresponding height profile. A red colored dot indicates a single Abl tyrosine kinase, whose size is below 3 nm, and a white colored dot represents aggregated proteins whose size is larger than 3 nm. (b) KPFM images of Abl tyrosine kinase with two different scanning speeds, 1.2 and 15 μm/s. (c) Surface potentials for Abl tyrosine kinase as a function of the lift scan height at a scanning speed of 1.2 μm/s. (d) KPFM image of individual Abl tyrosine kinase with a scanning speed of 1.2 μm/s and lift scan height of 5 nm and its corresponding surface potential profile. The inset indicates the tmAFM image of Abl tyrosine kinase which is able to confirm the single protein (red dot).

though the measured surface potential is usually affected by the scan range of ~100 nm (ref 36), which is much larger than the size of a single protein. In particular, the KPFM profile shows that a single protein is negatively charged and that a single protein possesses a larger amount of surface potential than the silicon substrate by ~25 mV (Figure 3a). The negative value of surface potential for protein kinase is consistent with the fact that the isolectric point of Abl tyrosine kinase is 5.86 (computed from ExPASy proteomics server, Swiss Institute of Bioinformatics)[37] that is smaller than the pH of a buffer solution (pH 7.5), which results in the negative quantity of the measured surface potential.[24] Furthermore, a noise error in the measured surface potential of the silicon substrate is <5 mV, which is much smaller than 25 mV, that is, the difference between surface potentials of Abl tyrosine kinase and silicon substrate, respectively. In general, the error in the measured surface potential can be significantly reduced by lowering the temperature[30] (*i.e.*, locking the thermal fluctuation of KPFM tip motion) and/or using a sharp KPFM tip.[38,39] Figure 3a confirms that KPFM is able to recognize a single protein on the substrate. Here, it should be noted that KPFM imaging requires a sample prepared in ambient conditions rather than an aqueous environment because the capacitance between the AFM tip and a sample is discharged in an aqueous environment,[30] which implies the restrictions of KPFM for imaging biological samples under physiological conditions.

Single-Molecule Recognition of Protein–Small-Molecule Interactions. For the proof-of-concept, we have taken into account both tmAFM and KPFM for imaging the individual Abl tyrosine kinases in the unbound state, ATP-bound state, and Imatinib-bound state. Figure 3a shows the tmAFM images of individual Abl tyrosine kinases in three states, and their corresponding tmAFM height profiles are presented in Figure 3b. Here, Abl tyrosine kinases in the Imatinib-bound state for both tmAFM imaging and KPFM imaging are prepared in such a way that Abl tyrosine kinases in buffer solution are reacted only with Imatinib, and then the sample is dried for imaging (for details, see Methods). The tmAFM height profiles of Abl tyrosine kinases in three different states provide evidence that the size of imaged Abl tyrosine kinases in three different states is invariant regardless of ligand binding such as ATP binding or Imatinib binding (Figure 3c). This indicates that the tmAFM imaging technique is unable to clearly distinguish protein kinases in the ATP-bound state from those in unbound states. This is attributed to the limited spatial resolution of tmAFM imaging such that small molecules such as ATP (MW = 499.52 Da) or Imatinib (MW = 598.7 Da) are too small to be imaged by

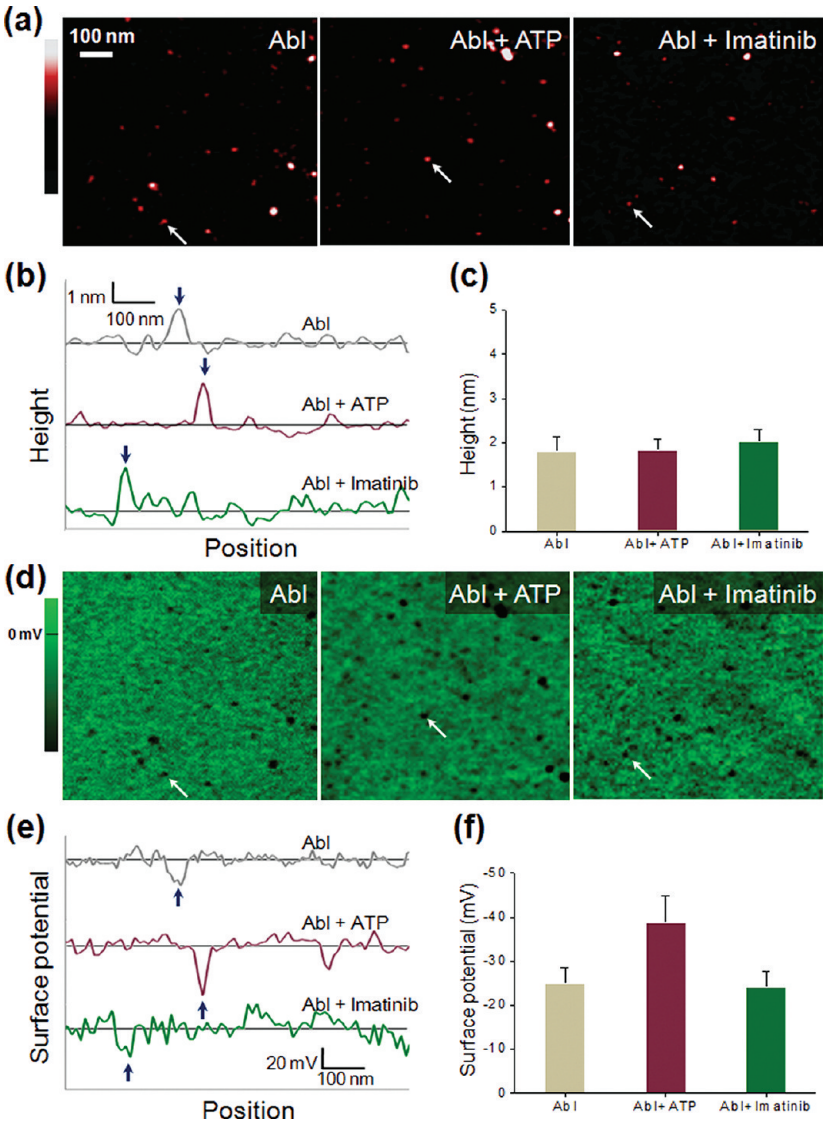

Figure 3. (a) Tapping-mode AFM images of Abl tyrosine kinases (marked as a white arrow) in unbound state (left), ATP-bound state (middle), and Imatinib-bound state (right). (b) AFM height profiles of Abl tyrosine kinase in unbound state (gray), ATP-bound state (purple), and Imatinib-bound state (green). (c) Average height of imaged tyrosine kinases in three different states. (d) KPFM images of Abl tyrosine kinases (marked as a white arrow) in unbound state (left), ATP-bound state (middle), and Imatinib-driven inhibition state (right). (e) Surface potential profiles of an Abl tyrosine kinase in three different states. (f) Average surface potential of imaged Abl tyrosine kinases in three different states.

tmAFM. On the other hand, KPFM imaging allows an identification of Abl tyrosine kinases in the ATP-bound state from those in the unbound state (Figure 3d). Specifically, the surface potential profiles show that ATP binding onto an Abl tyrosine kinase increases the magnitude of surface potential by ~25 mV presumably due to negative charges of ATP (Figure 3e,f). Moreover, in order to compare an Abl tyrosine kinase in the Imatinib-bound state with that in the ATP-bound state, we have also taken into account the KPFM imaging and the corresponding surface potential profile (Figure 3d,e). It is found that the surface potential of Abl tyrosine kinase in the Imatinib-bound state is almost similar to that of a pure Abl tyrosine kinase, which is attributed to the fact that Imatinib is electrically neutral and hence does not change the surface potential. This result suggests that the KPFM imaging technique enables the distinction of Abl tyrosine kinases in the Imatinib-bound state from those in the ATP-bound state when Abl tyrosine kinases are exposed to both ATP and Imatinib simultaneously.

Quantitative Analysis on Binding Affinities and Drug-Induced Inhibition. For quantitative characterization of binding affinities between Abl tyrosine kinase and small molecules such as ATP or Imatinib, we have considered >200 individual Abl tyrosine kinases in the unbound state, ATP-bound state, and inhibited state, which were imaged by KPFM. First, to characterize the binding affinity between Abl tyrosine kinase and ATP, let us consider >200 Abl tyrosine kinases in unbound state

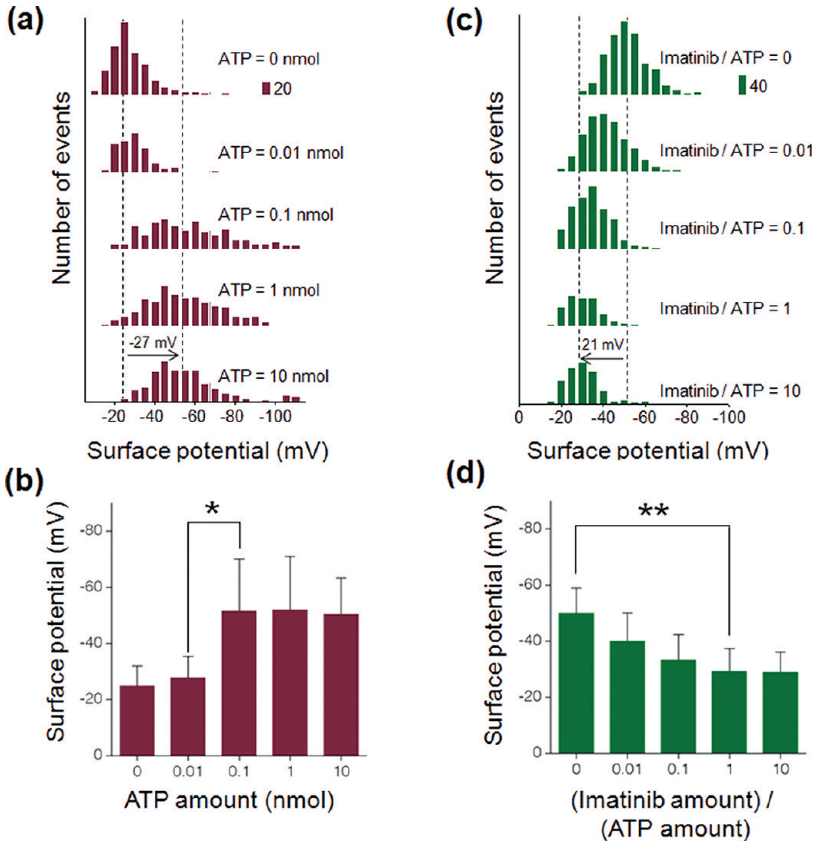

Figure 4. (a) Surface potential distribution for Abl tyrosine kinases, which are likely to be bound to ATP, as a function of ATP amount, and (b) their mean surface potentials (*$p < 0.0001$) are presented. (c) Surface potential distribution for Abl tyrosine kinases, which are likely to interact with either ATP or Imatinib, with respect to ratio of Imatinib amount to ATP amount denoted as (Imatinib amount)/(ATP amount), and (d) their mean surface potentials ($p < 0.0001$) are shown.**

and ATP-bound state. Here, samples were prepared such that Abl tyrosine kinases with the amount of 500 units (equivalent to 0.85 pmol) are reacted to ATP with different amounts ranging from 0.01 to 10 nmol in buffer solution, and then each sample containing Abl tyrosine kinases, which are likely to be bound to ATP, was disposed onto silicon substrate and subsequently dried for imaging.[26] As presented in Supporting Information (Figure S5), the size distribution of Abl tyrosine kinases remains constant regardless of ATP binding, which shows the limitation of the AFM imaging technique for label-free detection of ATP binding onto a single protein. However, as shown in Figure 4a, the probability distribution of surface potentials for Abl tyrosine kinases is shifted with respect to ATP amount. It is found that the probability distribution of the surface potential for ATP-bound protein kinase is broad, which is attributed to fact that the error range for measured surface potential is ± 5 mV. It is noted that the error range is still less than the measured surface potential for a protein (*i.e.*, $\sim$20 mV). Moreover, the broad distribution of the measured surface potential may also be attributed to the sample preparation that proteins are deposited onto a silicon substrate. When the proteins are deposited on the substrate, the relative orientation of a binding site with respect to the substrate for a protein may be quite different between deposited proteins, which may cause the broad distribution of surface potentials. If there are two distinct states such as an unbound state and ATP-bound state, the probability distribution may be bimodal, where each peak corresponds to either unbound or ligand-bound states, respectively. Though the surface potential distribution (shown in Figure 4a) resembles a Gaussian distribution due to the large standard deviation of measured surface potential, we can decompose the surface potential distribution into two distributions corresponding to two distinct states (such as unbound and ATP-bound states) as in a bimodal distribution (for details, see supplementary methods and Figure S6 in Supporting Information). This indicates that the surface potential distributions for ATP-bound protein kinases allow for quantifying the number of ATP-bound proteins and/or unbound proteins. In particular, the broad probability distribution $p_{eff}(E)$ of the surface potential for single proteins reacted with ATP molecules with an amount of 0.01 to 1 nmol can be represented in the form of $p_{eff}(E) = \alpha_u p_u(E) + \alpha_b p_b(E)$, where E is the surface potential, $p_u(E)$ is the surface potential distribution for single proteins at the unbound state, $p_b(E)$ is the surface potential distribution for single proteins reacted to ATP molecules with an amount of 10 nmol

TABLE 1. Fractions in Numbers for Tyrosine Kinases in Unbound State and ATP-Bound State (α_u and α_b) and Fractions in Numbers for Kinases in ATP-Bound State and Imatinib-Inhibited State (β_b and β_I) Are Suggested

binding experiment			inhibition experiment		
ATP amount (nmol)	α_u	α_b	Imatinib amount/ATP amount	β_b	β_I
0.01	0.836	0.164	0.01	0.642	0.358
0.1	0.4545	0.5455	0.1	0.2748	0.7252
1	0.0627	0.9373	1	0.1083	0.8912

(where all single proteins may be fully reacted to ATP molecules), α_u and α_b are the fractions in the numbers of proteins in the unbound state and ATP-bound state, respectively, that is $\alpha_u = 1 - \alpha_b$ and $0 \leq \alpha_u \leq 1$ (for details, see supplementary method). The binding efficacy for ATP binding onto Abl kinases with respect to ATP amount is summarized in Table 1. Figure 4b depicts the magnitude of mean surface potential for Abl tyrosine kinases as a function of ATP amount. It is clearly seen that mean surface potential increases with respect to ATP amount, implying that the number of Abl tyrosine kinases bound to ATP is likely to increase with respect to ATP amount. Moreover, we found that the mean surface potential of protein kinases in the ATP-bound state is saturated at an ATP amount of 0.1 nmol. It is suggested that KPFM enables the qualitative understanding of binding affinity between a protein and a small molecule. However, there is still a gap between the surface potential measured from KPFM and the binding affinities (and also activation energy) predicted from theory and simulations,[8,9] albeit there was an effort[23] to relate the measured surface potential to theoretical predictions on the surface charges of a protein. It is still required to bridge the gap between experimental observations and computational predictions on underlying binding mechanisms (see Discussion).

To characterize the Imatinib-driven inhibition of ATP binding onto Abl tyrosine kinase, we consider the measured surface potentials of >200 Abl tyrosine kinases that are exposed to both ATP and Imatinib simultaneously. Here, we prepared a sample such that the buffer solution contains Abl tyrosine kinases with 500 units, ATP molecules at 0.1 nmol, and Imatinib molecules with different amounts ranging from 0.001 to 1 nmol. Then, such buffer solution is dropped onto a silicon substrate and subsequently dried for KPFM imaging (see Methods). Figure 4c provides the probability distribution of surface potentials for Abl tyrosine kinases, which are likely to be reacted either of ATP or Imatinib, as a function of Imatinib amounts. As described earlier, at intermediate Imatinib amounts (denoted as [Imatinib]), the surface potential distribution can be fitted to the form of $p_{eff}(E) = \beta_b p_b(E) + \beta_I p_I(E)$, where $p_b(E)$ and $p_I(E)$ represent the surface potential distributions for ATP-bound state (*i.e.*, [Imatinib] = 0 nmol) and Imatinib-inhibited state (*i.e.*, [Imatinib] = 1 nmol), respectively, while β_b and β_I indicate the fractions in the numbers of ATP-bound state and Imatinib-inhibited state, respectively (see Figure S6 and Table 1). It is found that the probability distribution of surface potentials is shifted when the ratio of Imatinib with respect to that of ATP, denoted as [Imatinib amount]/[ATP], is increased. This indicates that number of Abl tyrosine kinases reacted with Imatinib is increasing with respect to [Imatinib]/[ATP]. The inhibition efficacy with respect to Imatinib amount is presented in Table 1. Figure 4d shows the magnitude of mean surface potential as a function of [Imatinib]/[ATP]. It is shown that an increase of [Imatinib]/[ATP] reduces the magnitude of mean surface potential, which highlights the quantitative description of Imatinib-induced inhibition of ATP binding. It is also seen that the mean surface potential saturates at [Imatinib]/[ATP amount] = 1, which indicates that it is probable for Imatinib (at [Imatinib]/[ATP] = 1) to effectively bind to all binding sites of Abl tyrosine. Here, it is presumed that all Abl tyrosine kinases are likely to be inhibited by Imatinib at [Imatinib]/[ATP] = 10 because the mean surface potential for Abl tyrosine kinases exposed to both Imatinib and at the ratio of 10 is almost close to that for pure Abl tyrosine kinases. With such a presumption, it is found that ~72% of Abl tyrosine kinases are likely to be inhibited by Imatinib at [Imatinib]/[ATP] = 0.1, which implies that Imatinib even in relatively low concentration effectively performs the inhibition of ATP binding.

Discussion. As delineated above, it is required to bridge KPFM-based observation and computational simulation (*e.g.*, molecular dynamics simulation)-based predictions in the underlying binding mechanism. In other words, KPFM can be regarded as a robust experimental tool that can validate the simulation-based predictions in the binding mechanism. In order to make connection between experimental observation and theories (and simulations), we have taken into account the kinetic theory, particularly two-state kinetic model,[40] along with Kramers' transition theory.[41−43] As shown in Figure 4 and Table 1, the surface potential of protein kinases with respect to ATP concentrations, which is measured from KPFM experiment, provides the

fractions in the numbers of ATP-bound kinases and unbound kinases. These quantities (*i.e.*, α_u and α_b) may be a relevant measure in order to study the binding mechanism. In particular, these quantities satisfy the kinetic equation for two-state kinetic model, given by[40]

$$\begin{bmatrix} d\alpha_u/dt \\ d\alpha_b/dt \end{bmatrix} = \begin{bmatrix} -k_b & k_u \\ k_b & -k_u \end{bmatrix} \begin{bmatrix} \alpha_u \\ \alpha_b \end{bmatrix} \quad (1)$$

where k_b represents the kinetic rate for transition from the unbound state to ligand-bound state, whereas k_u indicates the kinetic rate for transition from the ligand-bound state to unbound state. The solution to the kinetic equation depicted in eq 1 provides the fractions in the numbers of unbound (or ATP-bound) proteins in the form of

$$\begin{bmatrix} \alpha_u(t) \\ \alpha_b(t) \end{bmatrix} = \begin{bmatrix} k_u k^{-1} + k_b k^{-1}\exp(-kt) & k_b k^{-1}\{1 - \exp(-kt)\} \\ k_b k^{-1}\{1 - \exp(-kt)\} & k_b k^{-1} + k_u k^{-1}\exp(-kt) \end{bmatrix} \begin{bmatrix} \alpha_u(0) \\ \alpha_b(0) \end{bmatrix} \quad (2)$$

where $k = k_b + k_u$. In our experiment, the reaction time is sufficiently large enough to ensure the complete interactions between protein kinases and ligands (*e.g.*, ATPs). For this case (*i.e.*, $t \rightarrow \infty$), the fractions in numbers of unbound (or ligand-bound) kinases are given as

$$\lim_{t \rightarrow \infty} \alpha_u(t) = \frac{k_u}{k_u + k_b} \text{ and } \lim_{t \rightarrow \infty} \alpha_b(t) = \frac{k_b}{k_u + k_b} \quad (3)$$

Equation 3 clearly demonstrates that the quantities (*i.e.*, α_u and α_b) are correlated with the kinetic rates k_u and k_b. In other words, our KPFM experimental measurements can provide the equilibrium constant K (*i.e.*, $K = k_b/k_u$) such as $K = \alpha_b/\alpha_u$, where α_u and α_b can be estimated from KPFM measurements.

The equilibrium constant measured from KPFM experiment could be compared with the theoretical/computational predictions. Specifically, to analytically derive the equilibrium constant, we consider Kramers' transition theory[41−43] that enables the extraction of the kinetic rate (*i.e.*, k_b or k_u) from a presumed free energy landscape shown in Figure S7 in Supporting Information. Specifically, the kinetic rates k_b and k_u can be related to parameters that are relevant to describe the shape of the free energy landscape.[41−44]

$$k_u = \frac{\Omega_u \Omega_{ts}}{2\pi\gamma} \exp\left(-\frac{\Delta G_{u \rightarrow b}}{k_B T}\right) \text{ and } k_b = \frac{\Omega_b \Omega_{ts}}{2\pi\gamma} \exp\left(-\frac{\Delta G_{b \rightarrow u}}{k_B T}\right) \quad (4)$$

where Ω_u, Ω_{ts}, and Ω_b represent the vibrational frequencies at unbound state, transition state, and ligand-bound state, respectively, $\Delta G_{u \rightarrow b}$ is a free energy barrier that has to be overcome for transition from the unbound state to the ligand-bound state, $\Delta G_{b \rightarrow u}$ is a free energy barrier that has to be crossed over for transition from the ligand-bound state to the unbound state, and γ, k_B, and T indicate the frictional coefficient, Boltzmann's constant, and absolute temperature, respectively. Here, vibrational frequencies can be obtained from the shape of a free energy landscape such as $\Omega_u = G''(x_u)$, $\Omega_b = G''(x_b)$, and $\Omega_{ts} = G''(x_{ts})$, where $G(x)$ is a free energy landscape as a function of reaction coordinate x, while x_u, x_b, and x_{ts} indicate the reaction coordinates at the unbound state, ligand-bound state, and transition state, respectively, and prime represents the differentiation with respect to the reaction coordinate. From eqs 3 and 4, the equilibrium constant can be related to the parameters of a free energy landscape such as

$$K = \frac{\Omega_b}{\Omega_u} \exp\left(-\frac{\Delta G_{b \rightarrow u} - \Delta G_{u \rightarrow b}}{k_B T}\right) \quad (5)$$

As shown in eq 5, the vibrational frequencies (*i.e.*, Ω_b and Ω_u) affect the equilibrium constant, which consequently changes the fractions in the numbers of ligand-bound proteins (or unbound proteins). The equilibrium constant K that can be experimentally obtained from the measured surface potential distributions (*i.e.*, $K = \alpha_b/\alpha_u$) could be compared with the theoretical model that describes the equilibrium constant with respect to the free energy landscape (*e.g.*, eq 5). In particular, molecular dynamics (MD) simulations based on umbrella sampling[45] allow the extraction of free energy landscape for a protein and consequently the equilibrium constant. This implies that KPFM experiments may allow the validation of theoretical studies on the binding mechanism for a protein based on the comparison between equilibrium constants predicted from KPFM experiment and MD simulation. In addition, our KPFM measurements for identifying ligand binding onto a protein may be useful in validating the binding affinities between ligand and a protein predicted from computational simulations such as MD simulation.[8,9] For instance, the competitive interactions between various small molecules and a protein can be predicted from computational simulations, while such competitive interactions can be measured from our KPFM experiment. In summary, our KPFM may be extended with theory and computational simulations to gain a fundamental insight into the binding mechanism at single-molecule resolution.

CONCLUSION

In summary, we report a novel approach based on SPM technique, particularly KPFM imaging, which allows for identification of interactions between small molecules and tyrosine kinase (that is a target molecule for cancers[12]). It is noted that until recently the method has not been available, which can provide information of binding affinities at single-

molecule resolution; this information is essential for effective drug design. It is due to the limitation of existing methods such as label-free detection using nanoscale devices (*e.g.*, nanowire FET[10]) that exhibit the restrictive resolution. However, as described in this study, KPFM experiment is able to endow an insight into binding mechanism, which could be compared with that predicted from simulations (or theory) at single-molecule level. In the long run, our study can be further employed to validate the effectiveness of a designed molecule as a drug by measuring the binding affinities at single-molecule level. This implies that KPFM may be regarded as a single-molecule drug-screening toolkit capable of revealing an insight into the efficacy of designed drugs including nanomedicine. In addition, KPFM could be utilized for mapping various binding affinities between various molecular interactions such as protein−protein interactions; the mapping of these interactions may be useful in proteomics that can elucidate cellular signaling cascade or regulation of such signaling that determines the cellular functions or malfunctions.[46] Our study sheds light on KPFM as a single-molecule experimental toolkit that may be useful for future applications in nanomedicine, such as drug design and proteomics.

METHODS

Sample Preparation. We have used Abelson (Abl) tyrosine kinase (New England Biolabs, Beverly, MA), which was supplied in a frozen solution containing 100 nM NaCl, 50 mM HEPES (pH 7.5), 0.1 mM Na_2EDTA, 1 mM DTT, 0.01% Brij-35, and 50% glycerol. Such a solution is thawed at room temperature, and then 5 μL of solution (containing Abl tyrosine kinase) was dissolved into deionized water (pH 7.5) with its volume of 5 μL. This leads to buffer solution in which Abl tyrosine kinase was dissolved at a concentration of 50 units/μL. For tmAFM- and KPFM-based imaging, we dropped 2 μL of a buffer solution onto a silicon substrate, which was already cleansed using ethyl alcohol and deionized water, and then dried overnight. In addition, the prepared surface that includes the Abl kinases was gently rinsed with deionized water in order to remove the ions that can affect the surface potential profile of a sample.[26] Finally, the sample is dried for KPFM imaging.

For imaging of Abl tyrosine kinase in the ATP-bound state, we have prepared a solution in which Abl tyrosine kinases are reacted with ATP. Here, ATP (New England Biolabs, Beverly, MA) was supplied in sterile purified water adjusted to pH 7.0 using NaOH. Herein, the ATP concentration of the supplied solution is 10 mM, and then it is diluted with deionized water in order to have the specific ATP amounts of 0.01, 0.1, 1, and 10 nmol. Subsequently, two prepared solutions (*i.e.*, a solution containing Abl tyrosine kinases and the other to have ATP) were mixed over 5 h in order to guarantee the perfect reaction between Abl tyrosine kinases and ATP. Then, such a mixed solution was placed on the silicon substrate and dried overnight in a vacuum desiccator for tmAFM imaging. For KPFM imaging, as described above, the surface on which Abl kinases are deposited is gently rinsed with deionized water in order to eliminate the ions on the substrate.

For SPM imaging of Abl tyrosine kinases in the Imatinib-bound state, we have prepared a solution to contain Abl tyrosine kinase reacted to Imatinib. In order to prepare a solution containing Imatinib, we have extracted the Imatinib from Gleevec (Novartis Co., USA) as follows: one Gleevec tablet was broken and grinded for solubilization in ethyl acetate. Then, Imatinib solution was purified three times using buffer solution, and then the organic phase was dried for the binding inhibition experiment. Herein, the chemical structure of obtained Imatinib powder was confirmed by ^{1}H NMR (400 MHz, CD_3OD): δ = 9.28 (−NH−), 8.36 (−CH═; from pyridine), 8.46 (−CH═; from pyrimidine), 7.92, 7.54, 7.48, 7.40, 7.35, 7.25 (−CH═), 6.93, 3.63 ($-CH_2-$), 2.46 ($-CH_2-$; from piperazine), 2.31 ($-CH_3-$), 2.23 ($-CH_3-$; from methylpiperazine). Such prepared Imatinib solution was mixed with the prepared solution containing Abl tyrosine kinase in order to obtain the buffer solution in which Abl tyrosine kinases are likely to be bound to Imatinib. Finally, such buffer solution was dropped onto the substrate and dried for imaging.

For imaging and quantitative analysis of Imatinib-induced inhibition, we have separately prepared two different solutions, one of which has ATP molecules and the other contains the Imatinib molecules. Then a prepared solution containing Abl tyrosine kinase was mixed with two aforementioned solutions in order to have the buffer solution, in which Abl tyrosine kinases are likely to be reacted with either of ATP or Imatinib. Then, such a buffer solution was disposed onto the substrate and then dried overnight. Finally, the surface on which Abl kinases are disposed was rinsed with deionized water (to remove the ions on the substrate) and dried for imaging and further analysis.

Tapping-Mode AFM Imaging. We have used Innova (Veeco Inc., Santa Barbara, CA) with a Nanodrive controller (Veeco Inc.) for tapping-mode AFM (tmAFM) imaging. The tmAFM imaging was implemented using closed loop scanner, which allows one to obtain the reproducible image of biomolecules regardless of rescanning. For tmAFM imaging, we have utilized a SCM-PIT cantilever tip (Veeco Inc., Santa Barbara, CA) that exhibits the resonance of ~75 kHz and tip radius of ~20 nm. All tmAFM images were obtained based on scanning area ranging from 800 nm × 800 nm to 1500 nm × 1500 nm and scanning speed of 0.8 Hz, unless otherwise specified. All images were produced by SPM Lab Analysis software V7.0 (Veeco Inc., Santa Barbara, CA).

Physical Concept of KPFM. The key concept of KPFM is attributed to Lord Kelvin,[27] who first suggested the method to measure the differences in the work functions (*i.e.*, surface potentials) of a substrate and a layer. Here, a substrate and layer constitutes the capacitance. The periodic vibration in distance between substrate and layer is induced, which is referred to as "vibrating capacitance method", in order to measure the differences in the work functions. On the basis of the concept suggested by Lord Kelvin, an AFM tip (acting as a layer) is vibrating so as to induce the periodic vibration in the distance between sample (acting as substrate) and AFM tip. The force exerted in an AFM tip due to surface potential difference between sample and AFM tip is given by[30]

$$F = \left(\frac{\pi\varepsilon_0 R}{d}\right)\left[V_{ac}{}^2 + V_{ac}\Phi \sin \omega t + \frac{1}{2}V_{ac}{}^2(1 - \cos \omega_{ac} t)\right] \quad (6)$$

where ε_0 is the permittivity between the AFM tip and sample, R is the radius of an AFM tip, d is the distance between AFM tip and sample, V_{ac} is the magnitude of applied ac voltage, ω is the resonant frequency of an AFM tip, ω_{ac} is the frequency of applied ac voltage, and Φ is the surface potential difference between the AFM tip and the sample. In general, KPFM techniques measure the force exerted due to surface potential difference, and then the surface potential difference can be estimated from the physical concept depicted in eq 6.

KPFM Imaging. KPFM images were obtained based on lift-mode, where tip bias potential is oscillating at the resonant frequency of a cantilever. In general, before implementation of KPFM imaging, we conducted tmAFM imaging that helps to

know the parameters for KPFM imaging. Subsequently, we consider the line scanning (using tmAFM imaging) in order to set up the parameters for KPFM imaging. In order to tune the control feedback parameters (*e.g.*, phase, proportion, and integral gains), we have checked KPFM error images, and then feedback parameters were adjusted. Finally, for KPFM imaging, a cantilever tip was moved along the *z*-axis (perpendicular to sample surface) with prescribed lift height, and 4 V alternating current (ac) amplitude was applied to the tip. Here, the sample was grounded using a carbon tape and silver paste (Dotite, Japan). This ground system enables us to reduce the error signal as well as charge-up phenomenon. All KPFM images were produced with SPM Lab Analysis software V7.0.

Acknowledgment. The authors appreciate the fruitful discussions with Dr. T. Mueller at Veeco Inc. (Santa Barbara, CA, USA). Moreover, a helpful comment from pharmacist, Mr. J. Kwon, is also gratefully acknowledged. This work was supported by the National Research Foundation of Korea (NRF) under Grant Nos. NRF-2008-313-D00031, NRF-2010-0009428, NRF-2010-0026223, NRF-2008-0059438, and M10755020001-7N5502-00110.

Supporting Information Available: Supplementary method in the data analysis of measured surface potentials and their distribution is described. Supplementary results on the dependence of KPFM imaging on experimental parameters such as scanning speed, scan height, and dual frequency mode are presented. Moreover, the size distributions of imaged proteins (in unbound state and ATP-bound state) are also provided. This material is available free of charge *via* the Internet at http://pubs.acs.org.

REFERENCES AND NOTES

1. Hanahan, D.; Weinberg, R. A. The Hallmarks of Cancer. *Cell* **2000**, *100*, 57–70.
2. Benson, J. D.; Chen, Y.-N. P.; Cornell-Kennon, S. A.; Dorsch, M.; Kim, S.; Leszczyniecka, M.; Sellers, W. R.; Lengauer, C. Validating Cancer Drug Targets. *Nature* **2006**, *441*, 451–456.
3. Bilanges, B.; Torbett, N.; Vanhaesebroeck, B. Killing Two Kinase Families with One Stone. *Nat. Chem. Biol.* **2008**, *4*, 648–649.
4. Wagner, K.; Moolenaar, G.; van Noort, J.; Goosen, N. Single-Molecule Analysis Reveals Two Separate DNA-Binding Domains in the *Escherichia coli* Uvra Dimer. *Nucleic Acids Res.* **2009**, *37*, 1962–1972.
5. Huang, D.; Zhou, T.; Lafleur, K.; Nevado, C.; Caflisch, A. Kinase Selectivity Potential for Inhibitors Targeting the ATP Binding Site: A Network Analysis. *Bioinformatics* **2010**, *26*, 198–204.
6. Lehn, J.-M. Perspectives in Supramolecular Chemistry—From Molecular Recognition towards Molecular Information Processing and Self-Organization. *Angew. Chem., Int. Ed. Engl.* **1990**, *29*, 1304–1319.
7. Buehler, M. J.; Yung, Y. C. Deformation and Failure of Protein Materials in Physiologically Extreme Conditions and Disease. *Nat. Mater.* **2009**, *8*, 175–188.
8. Hummel, P.; Vaidehi, N.; Floriano, W. B.; Hall, S. E.; Goddard, W. A. Test of the Binding Threshold Hypothesis for Olfactory Receptors: Explanation of the Differential Binding of Ketones to the Mouse and Human Orthologs of Olfactory Receptor 912-93. *Protein Sci.* **2005**, *14*, 703–710.
9. Huang, Z.; Wong, C. F. Conformational Selection of Protein Kinase A Revealed by Flexible-Ligand Flexible-Protein Docking. *J. Comput. Chem.* **2009**, *30*, 631–644.
10. Wang, W. U.; Chen, C.; Lin, K.-h.; Fang, Y.; Lieber, C. M. Label-Free Detection of Small-Molecule–Protein Interactions by Using Nanowire Nanosensors. *Proc. Natl. Acad. Sci. U.S.A.* **2005**, *102*, 3208–3212.
11. Strausberg, R. L.; Schreiber, S. L. From Knowing to Controlling: A Path from Genomics to Drugs Using Small Molecule Probes. *Science* **2003**, *300*, 294–295.
12. Sebolt-Leopold, J. S.; English, J. M. Mechanisms of Drug Inhibition of Signalling Molecules. *Nature* **2006**, *441*, 457–462.
13. Allison, D. P.; Hinterdorfer, P.; Han, W. Biomolecular Force Measurements and the Atomic Force Microscope. *Curr. Opin. Biotechnol.* **2002**, *13*, 47–51.
14. Dong, M.; Husale, S.; Sahin, O. Determination of Protein Structural Flexibility by Microsecond Force Spectroscopy. *Nat. Nanotechnol.* **2009**, *4*, 514–517.
15. Engel, A.; Gaub, H. E. Structure and Mechanics of Membrane Proteins. *Annu. Rev. Biochem.* **2008**, *77*, 127–148.
16. Engel, A.; Muller, D. J. Observing Single Biomolecules at Work with the Atomic Force Microscope. *Nat. Struct. Mol. Biol.* **2000**, *7*, 715–718.
17. Wong, O. K.; Guthold, M.; Erie, D. A.; Gelles, J. Interconvertible Lac-Repressor DNA Loops Revealed by Single-Molecule Experiments. *PLoS Biol.* **2008**, *6*, e232.
18. Eom, K.; Park, H. S.; Yoon, D. S.; Kwon, T. Nanomechanical Resonators and Their Applications in Biological/Chemical Detection: Nanomechanics Principles. *Phys. Rep.* **2011**, *503*, 115–163.
19. Kwon, T.; Park, J.; Yang, J.; Yoon, D. S.; Na, S.; Kim, C.-W.; Suh, J.-S.; Huh, Y.-M.; Haam, S.; Eom, K. Nanomechanical *In Situ* Monitoring of Proteolysis of Peptide by Cathepsin B. *PLoS ONE* **2009**, *4*, e6248.
20. Braun, T.; Ghatkesar, M. K.; Backmann, N.; Grange, W.; Boulanger, P.; Letellier, L.; Lang, H.-P.; Bietsch, A.; Gerber, C.; Hegner, M. Quantitative Time-Resolved Measurement of Membrane Protein–Ligand Interactions Using Microcantilever Array Sensors. *Nat. Nanotechnol.* **2009**, *4*, 179–185.
21. Husale, S.; Persson, H. H. J.; Sahin, O. DNA Nanomechanics Allows Direct Digital Detection of Complementary DNA and MicroRNA Targets. *Nature* **2009**, *462*, 1075–1078.
22. Cheran, L. E.; Chacko, M.; Zhang, M. Q.; Thompson, M. Protein Microarray Scanning in Label-Free Format by Kelvin Nanoprobe. *Analyst* **2004**, *129*, 161–168.
23. Chun, D. W.; Hwang, K. S.; Eom, K.; Lee, J. H.; Cha, B. H.; Lee, W. Y.; Yoon, D. S.; Kim, T. S. Detection of the Au Thin-Layer in the Hz per Picogram Regime Based on the Microcantilevers. *Sens. Actuators, A* **2006**, *135*, 857–862.
24. Sinensky, A. K.; Belcher, A. M. Label-Free and High-Resolution Protein/DNA Nanoarray Analysis Using Kelvin Probe Force Microscopy. *Nat. Nanotechnol.* **2007**, *2*, 653–659.
25. Zhou, D.; Sinniah, K.; Abell, C.; Rayment, T. Label-Free Detection of DNA Hybridization at the Nanoscale: A Highly Sensitive and Selective Approach Using Atomic-Force Microscopy. *Angew. Chem., Int. Ed.* **2003**, *42*, 4934–4937.
26. Leung, C.; Kinns, H.; Hoogenboom, B. W.; Howorka, S.; Mesquida, P. Imaging Surface Charges of Individual Biomolecules. *Nano Lett.* **2009**, *9*, 2769–2773.
27. Lord, K. Contact Electricity of Metals. *Philos. Mag.* **1898**, *46*, 82–120.
28. Lee, I.; Greenbaum, E.; Budy, S.; Hillebrecht, J. R.; Birge, R. R.; Stuart, J. A. Photoinduced Surface Potential Change of Bacteriorhodopsin Mutant D96n Measured by Scanning Surface Potential Microscopy. *J. Phys. Chem. B* **2006**, *110*, 10982–10990.
29. Druker, B. J.; Lydon, N. B. Lessons Learned from the Development of an Abl Tyrosine Kinase Inhibitor for Chronic Myelogenous Leukemia. *J. Clin. Invest.* **2000**, *105*, 3–7.
30. Nonnenmacher, M.; Boyle, M. P. O.; Wickramasinghe, H. K. Kelvin Probe Force Microscopy. *Appl. Phys. Lett.* **1991**, *58*, 2921–2923.
31. Jacobs, H. O.; Leuchtmann, P.; Homan, O. J.; Stemmer, A. Resolution and Contrast in Kelvin Probe Force Microscopy. *J. Appl. Phys.* **1998**, *84*, 1168–1173.
32. Fujihira, M. Kelvin Probe Force Microscopy of Molecular Surfaces. *Annu. Rev. Mater. Sci.* **1999**, *29*, 353.
33. Gao, P.; Cai, Y. Label-Free Detection of the Aptamer Binding on Protein Patterns Using Kelvin Probe Force Microscopy. *Anal. Bioanal. Chem.* **2009**, *394*, 207–214.
34. Mueller, T. Private communication.
35. Hansma, P. K.; Schitter, G.; Fantner, G. E.; Prater, C. High-Speed Atomic Force Microscopy. *Science* **2006**, *314*, 601–602.
36. Liscio, A.; Palermo, V.; Samor, P. Probing Local Surface Potential of Quasi-One-Dimensional Systems: A Kpfm Study of P3ht Nanofibers. *Adv. Funct. Mater.* **2008**, *18*, 907–914.

37. http://expasy.org/tools/pi_tool.html.
38. Sadewasser, S.; Leendertz, C.; Streicher, F.; Lux-Steiner, M. C. The Influence of Surface Topography on Kelvin Probe Force Microscopy. *Nanotechnology* **2009**, *20*, 505503.
39. Douheret, O.; Anand, S.; Glatzel, T.; Maknys, K.; Sadewasser, S. Characterization of Quantum Wells by Cross-Sectional Kelvin Probe Force Microscopy. *Appl. Phys. Lett.* **2004**, *85*, 5245–5247.
40. Zwanzig, R. Two-State Models of Protein Folding Kinetics. *Proc. Natl. Acad. Sci. U.S.A.* **1997**, *94*, 148–150.
41. Kramers, H. A. Brownian Motion in a Field of Force and the Diffusion Model of Chemical Reactions. *Physica* **1940**, *7*, 284–304.
42. Bell, G. I. Models for the Specific Adhesion of Cells to Cells. A Theoretical Framework for Adhesion Mediated by Reversible Bonds between Cell Surface Molecules. *Science* **1978**, *200*, 618–627.
43. Hanggi, P.; Talkner, P.; Michal, B. Reaction-Rate Theory: Fifty Years after Kramers. *Rev. Mod. Phys.* **1990**, *62*, 251.
44. Garg, A. Escape-Field Distribution for Escape from a Metastable Potential Well Subject to a Steadily Increasing Bias Field. *Phys. Rev. B* **1995**, *51*, 15592.
45. McCammon, J. A.; Harvey, S. C. *Dynamics of Proteins and Nucleic Acids*; Cambridge University Press: Cambridge, 1987.
46. Spiller, D. G.; Wood, C. D.; Rand, D. A.; White, M. R. H. Measurement of Single-Cell Dynamics. *Nature* **2010**, *465*, 736–745.